Spectroscopic study of globular clusters in the halo of M31 with the Xinglong 2.16 m telescope [*]

Zhou Fan[1,2], Ya-Fang Huang[1,2], Jin-Zeng Li[1,2], Xu Zhou[1,2], Jun Ma[1,2], Hong Wu[1,2], Tian-Meng Zhang[1,2] and Yong-Heng Zhao[1,2]

[1] National Astronomical Observatories, Chinese Academy of Sciences, Beijing 100012, China; *zfan@bao.ac.cn*
[2] Key Laboratory of Optical Astronomy, National Astronomical Observatories, Chinese Academy of Sciences, Beijing 100012, China

Abstract We present spectroscopic observations for 11 confirmed globular clusters (GCs) of M31 with the OMR spectrograph on the 2.16 m telescope at the Xinglong site of National Astronomical Observatories, Chinese Academy of Sciences. Nine of our sample clusters are located in the halo of M31 and the most remote one is out to a projected radius of 78.75 kpc from the galactic center. For all our sample clusters, we measured the Lick absorption-line indices and radial velocities. It is noted that most GCs in our sample are distinct from the HI rotation curve of galaxy M31, especially for B514, MCGC5, H12 and B517, suggesting that most of our sample clusters do not have a kinematic association with the star-forming young disk of the galaxy. We separately fitted the absorption line indices from the updated stellar population model of Thomas et al. with two different tracks of Cassisi and Padova, by applying the χ^2-minimization method. The fitting results show that all our sample clusters are older than 10 Gyr, and metal-poor ($-2.38 \leq$ [Fe/H] ≤ -0.91 dex). After merging the spectroscopic metallicity of our work with the previously published ones, we extended the cluster sample out to a projected radius of 117 kpc from the galaxy's center. We found the metallicity gradient exists for all the confirmed clusters with a slope of -0.028 ± 0.001 dex kpc^{-1}. However, the slope turns out to be -0.018 ± 0.001 dex kpc^{-1} for all the halo clusters, which is much shallower. If we only consider the outer halo clusters with $r_{\rm p} > 25$ kpc, the slope becomes -0.010 ± 0.002 dex kpc^{-1} and if one cluster G001 is excluded from the outer halo sample, the slope is -0.004 ± 0.002 dex kpc^{-1}. Thus, we conclude that the metallicity gradient for M31's outer halo clusters is not significant, which agrees well with previous findings.

Key words: galaxies: individual (M31) — galaxies: star clusters — globular clusters: general — star clusters: general

1 INTRODUCTION

Galactic formation and evolutionary scenarios remain among the most important outstanding problems in contemporary astrophysics (Perrett et al. 2002). One way to better understand these questions is through detailed studies of globular clusters (GCs). These objects are often considered fossils of galactic formation and evolution processes, since they formed at the very early stages of their host galaxies' lifecycles (Barmby et al. 2000). GCs are usually densely packed, gravitationally bound spherical systems containing several thousand to approximately one million stars. Thus, they can be detected from great distances and are suitable as probes for studying the properties of extragalactic systems.

Located at a distance of approximately 780 kpc (Stanek & Garnavich 1998; Macri et al. 2001; McConnachie et al. 2005), M31 is the nearest and largest spiral galaxy in our Local Group. It contains a large number of GCs and is considered an ideal laboratory for studies of star clusters in external galaxies. Barmby & Huchra (2001) estimated the total number of GCs to be 460 ± 70, while Perina et al. (2010) arrived at ~ 530. Both of these estimates yield much larger numbers than for the GCs in our Galaxy. However, from the observational evidence collected to date (see, e.g., Rich et al. 2005), the M31 GCs and their Galactic counterparts reveal some striking similarities (Fusi Pecci et al. 1994; Djorgovski et al. 1997; Barmby et al. 2002). Based on survey data from the Canada-France-Hawaii Telescope (CFHT) and the Wide Field Camera on the Isaac Newton Telescope (INT), Huxor (2006) concluded that M31 and the Milky Way are more similar than previously thought. However, Hammer et al. (2007) compared our Galaxy and M31 to the local disk galaxies within the same mass range and found that the Milky Way is an exceptional disk galaxy which did not undergo any significant merging for the last 10 Gyr, so it lacks stellar mass, angular momentum, disk radius and metallicity of stars in the outskirts while M31 is a typical disk galaxy which is shaped by relatively recent merging. This may explain why there are more GCs in M31 than in our Galaxy, by a factor of three, since the merging could lead to the formation of GCs. Later, Yin et al. (2009) found that the two galaxies are similar in their radial profiles of star formation rate, gas profiles and stellar metallicity distributions along the disk by studying the chemical evolution history of the two galaxies. The authors concluded that the star formation efficiency of the M31 disk is twice as high as that in our Galaxy. Hou et al. (2009) also compared the two disk galaxies and concluded that the Milky Way disk contains more gas and a higher star formation rate than M31. The authors also find that the scaled abundance gradients are similar for the two galaxies. These recent works could provide useful clues that can explain the similarities and differences between the two GC systems. Therefore, studying the properties of the GCs in M31 not only improves our understanding of the formation and structure of our nearest large neighbor, but also of our own Galaxy.

A large number of halo GCs in M31 have recently been discovered. They are important for studying the formation history of M31 and its dark matter content. Huxor et al. (2004) discovered nine previously unknown GCs in the halo of M31 using the INT survey. Subsequently, Huxor et al. (2005) found three new, extended GCs in the halo of M31, which have characteristics between typical GCs and dwarf galaxies. Mackey et al. (2006) reported four extended, low-surface-brightness clusters in the halo of M31 based on the *Hubble Space Telescope*/Advanced Camera for Surveys (ACS) imaging. They are structurally very different from typical M31 GCs. However, their old and metal-poor characteristics are similar to those of typical GCs. Huxor (2006) discovered 40 new GCs in the halo of M31 (out to 100 kpc from the galactic center) based on INT and CFHT imaging. Some of them are also very extended. These extended star clusters in the M31 halo are very similar to the diffuse star clusters (DSCs) associated with early-type galaxies in the Virgo Cluster reported by Peng et al. (2006) based on the ACS Virgo Cluster survey. However, it seems that DSCs are usually fainter than typical GCs. Mackey et al. (2007) reported 10 outer-halo GCs in M31, at ~ 15 kpc to 100 kpc from the galactic center. Eight of these were newly discovered based on deep ACS imaging. The halo GCs in their sample are very bright, compact and metal poor, and therefore are quite different from

their counterparts in our Galaxy. Ma et al. (2010) constrained the age, metallicity, reddening and distance modulus of B379, which is located in the halo of M31, with the SSP model and photometry.

In this paper, we will present our new observations of a sample of new GCs, most of which are located far from the galaxy center. This allows us to be able to study the properties of the M31 outer halo in more detail. The paper is organized as follows. In Section 2 we describe how we selected our sample of M31 GCs and their spatial distribution. In Section 3, we report the spectroscopic observations with the 2.16 m telescope at the Xinglong site and the data reductions from which the radial velocities and Lick line indices are measured. Subsequently, in Section 4, we derive the ages and metallicities of GCs with χ^2-minimization fitting. We also discuss our final results on the metallicity distribution in the M31 halo. We give our summary in Section 5.

2 SAMPLE SELECTION

We selected the sources from the Revised Bologna Catalog of M31 globular clusters and candidates (RBC v.4, available from *http://www.bo.astro.it/M31*; Galleti et al. 2004, 2006, 2007, 2009), which is the latest and most comprehensive M31 GC catalog to date. It contains 2045 objects, including 663 confirmed star clusters, 604 cluster candidates and 778 other objects that were initially thought to be GCs but later proved to be stars, asterisms, galaxies or HII regions. In fact, many of the halo clusters were from Mackey et al. (2007), who reported 10 GCs in the outer halo of M31 from their deep ACS images, of which eight were detected for the first time (for details see Sect. 1). In our work, our sample clusters are completely selected from RBC v.4. We selected the confirmed, bright (< 17 mag in the V band) clusters located far from the galaxy center, where the local background is not too bright to observe. Finally, we selected 11 bright confirmed clusters in our sample and most of them are located in the halo of the galaxy. Although some of our sample clusters have previous spectroscopic observations by some authors, actually those clusters lack comprehensive spectroscopic information. In other words, they only have radial velocities, [Fe/H], [α/Fe] or age information. Therefore it is necessary to systematically observe the spectra of our sample clusters and study age and metallicity in detail.

The information on our sample GCs is listed in Table 1, including coordinates, projected radii, V-band magnitudes and age estimates. All the coordinates (Cols. (2) and (3)) and V-band magnitudes (Col. (5)) are from RBC v.4 except the V mag of EXT8 which was derived from $ugriz$ photometry of Peacock et al. (2010) with the transformation equation of Jester et al. (2005) since the V mag of EXT8 is not provided in RBC v.4. The projected radii from the galaxy center $r_{\rm p}$ (Col. (4))

Table 1 Parameters of Our Sample GCs

ID	R.A. (J2000)	Dec. (J2000)	$r_{\rm p}$ (kpc)	V (mag)	Age	References for ages[b]
(1)	(2)	(3)	(4)	(5)	(6)	(7)
MCGC2	00:29:44.90	+41:13:09.8	33.47	16.98	old	P
MCGC3	00:30:27.30	+41:36:20.4	31.88	16.31	old	P
B514	00:31:09.90	+37:53:59.7	55.39	15.76	> 10 Gyr	G
MCGC5	00:35:59.73	+35:41:03.8	78.73	16.09	old	P
B298	00:38:00.23	+40:43:55.9	14.28	16.59	old	C
H12	00:38:03.85	+37:44:00.6	50.03	16.47		
B019	00:40:52.52	+41:18:53.4	4.84	14.93	old	C
B020	00:40:55.26	+41:41:25.2	7.42	14.91	interm / old	P, C
B023	00:41:01.18	+41:13:45.7	4.46	14.22	old	P, C
EXT8	00:53:14.51	+41:33:24.7	27.27	15.54[a]		
B517	00:59:59.91	+41:54:06.6	45.08	16.08		

Notes: $r_{\rm p}$ refers to the projected radius from the center of the galaxy. [a] is derived from $ugriz$ photometry of Peacock et al. (2010) with the transformation equation of Jester et al. (2005). [b] P: age estimates from Peacock et al. (2010); C: from Caldwell et al. (2009); G: from Galleti et al. (2005).
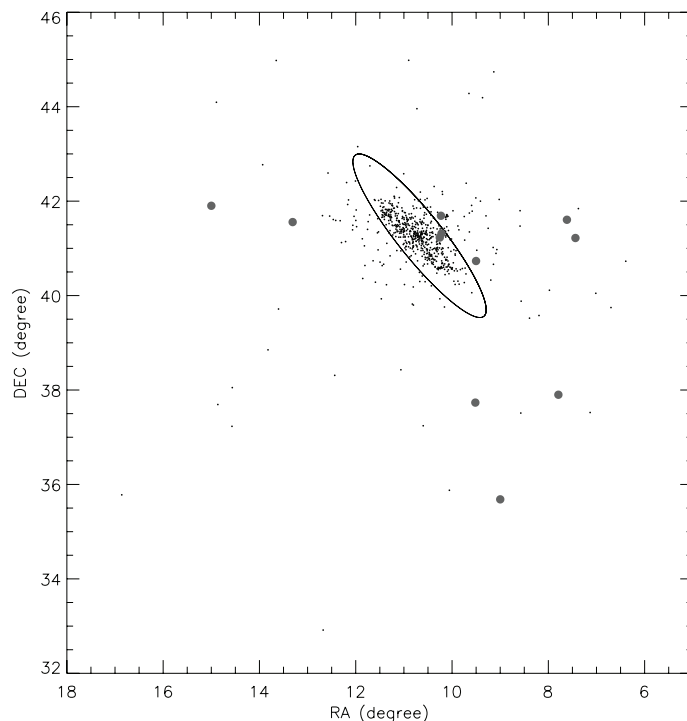
Fig. 1 Spatial distribution of our sample GCs (*filled circles*) and all the confirmed GCs from RBC v.4 (*points*). The large ellipse is the M31 disk/halo boundary as defined by Racine (1991).

were calculated with M31 center coordinates 00:42:44.31, +41:16:09.4 (Perrett et al. 2002), PA $= 38°$ and distance $= 785$ kpc (McConnachie et al. 2005). The ages (Col. (6)) are from a number of previous works: Peacock et al. (2010) by using the Sloan Digital Sky Survey (SDSS) and 2MASS photometric colors; Caldwell et al. (2009) by using the 6.5 m MMT Hectospec spectral line indices and HST CMD fittings; and Galleti et al. (2005) by comparing the line indices with the prediction models.

We show the spatial distribution of our sample GCs and all the confirmed GCs from RBC v.4 in Figure 1. The large ellipse is the M31 disk/halo boundary as defined by Racine (1991). Note that most of our sample is located in the halo of M31 except B019 and B023, which are very close to each other with a distance of ~ 5.5 arcmin. Thus, most of the GCs in our sample are halo GCs in M31, which can help us to access the nature of the galaxy's halo.

3 OBSERVATIONS AND DATA REDUCTION

Our low-resolution spectroscopic observations were all taken at the 2.16 m optical telescope at the Xinglong Site, which is part of the National Astronomical Observatories, Chinese Academy of Sciences (NAOC), 2010 September 10–13. An OMR (Optomechanics Research Inc.) spectrograph and a PI 1340×400 CCD detector were used during this run with a dispersion of 200 Å mm^{-1}, 4.8 Å pixel^{-1}, and a 3.0″slit. Exposures of 3×1800 s were taken with seeing typically $\sim 2.5″$. Our spectra cover the wavelength range of $3500 - 8100$ Å at 4 Å resolution. All our spectra have $S/N \geq 40$.

Table 2 Radial Velocities V_r of Our Sample GCs
and the Previous Results

ID (1)	This Work (2)	RBC v.4 (3)
MCGC2	-586.87 ± 39.98	
MCGC3	-416.46 ± 14.01	
B514	-429.42 ± 20.24	-458 ± 23
MCGC5	-417.55 ± 25.03	
B298	-648.50 ± 16.67	-539 ± 12
H12	-412.51 ± 33.05	
B019	-149.83 ± 22.91	-224 ± 2
B020	-231.87 ± 26.48	-351 ± 1
B023	-348.44 ± 21.30	-451 ± 5
EXT8	-104.55 ± 7.32	-154 ± 30
B517	-267.47 ± 20.73	-272 ± 54

The spectroscopic data were reduced following standard procedures using the NOAO Image Reduction and Analysis Facility (IRAF, version 2.11) software package. The CCD reduction includes bias and flat-field correction, as well as cosmic-ray removal. Wavelength calibration was performed based on helium/argon lamps exposed at both the beginning and the end of the observations each night. Flux calibration of all spectra was performed based on observations of at least two of the KPNO spectral standard stars (Massey et al. 1988) per night. The atmospheric extinction was corrected using the mean extinction coefficients measured at Xinglong by the Beijing-Arizona-Taiwan-Connecticut (BATC) multicolor sky survey (H. J. Yan 1995, priv. comm.).

Before we measured the Lick absorption line indices, the heliocentric radial velocities V_r were obtained by fitting the absorption lines of our spectra with templates of various radial velocities. The typical internal velocity errors of a single measurement are ~ 20 km s^{-1}. The estimated radial velocities V_r with their associated uncertainties (Col. (2)) are listed in Table 2. The published radial velocities V_r (Col. (3)) are also listed for comparisons. It can be seen that our measurements agree well with those listed in RBC v.4. At least, we cannot see significant differences between our measurements and the published values.

Similar to Galleti et al. (2005, 2006) and Caldwell et al. (2009), we plotted the radial velocity V_r (corrected for the systemic velocity of M31) versus the projected distance along the major axis (X) in Figure 2. The left panel is for all the confirmed clusters while the right panel is for the halo clusters which are defined in Figure 1. The small points are the published measurements from RBC v.4 while the filled circles with errors are the measurements in our work. Since Carignan et al. (2006) calculated the HI rotation curve of M31 out to ~ 35 kpc with the observation results of the Effelsberg and Green Bank 100 m telescopes, the HI rotation curve of galaxy M31 was over-plotted in Figure 2 with a continuous line. It can be seen that both the halo clusters and most of our sample clusters do not follow the disk mean velocity curve very well, especially for B514, MCGC5, H12 and B517, suggesting that they do not have kinematic association with the young star-forming disk of M31.

Subsequently, all the spectra were shifted to zero radial velocity and degraded to the wavelength dependent Lick resolution with a variable-width Gaussian kernel following the definition of Worthey & Ottaviani (1997), i.e. 11.5 Å at 4000 Å, 9.2 Å at 4400 Å, 8.4 Å at 4900 Å, 8.4 Å at 5400 Å and 9.8 Å at 6000 Å. Thus, we measured all the 25 types of Lick indices strictly by using the parameters and formulae from Worthey et al. (1994) and Worthey & Ottaviani (1997). The uncertainty of each index was estimated based on the analytic formulae (11)−(18) of Cardiel et al. (1998). All the Lick absorption line index measurements and 1σ errors are listed in Table 3.

As an example, Figure 3 shows the reduced spectroscopy of our sample GC B023, with all the Lick absorption line index bandpasses marked. The spectrum has been degraded and shifted to the zero radial velocity as described above. Actually, from the definitions of line indices of CN1
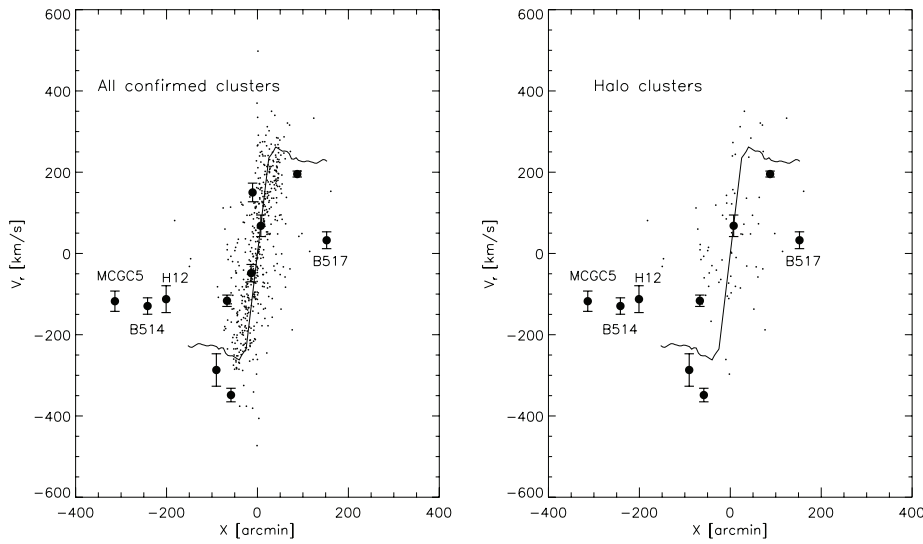
Fig. 2 Radial velocity V_r (corrected for the systemic velocity of M31) as a function of the projected distance along the major axis (X) in arcmin for all the confirmed clusters (*left*) and the halo clusters (*right*). The solid line is the HI rotation curve of the galaxy from Carignan et al. (2006). The filled circles with errors are the GCs from our sample while the small points are the velocity from the RBC v.4 catalog. It is easy to find that both the halo clusters and most of our sample clusters are distinct from the HI rotation curve of the galaxy, implying that they do not have kinematic association with the young star-forming disk of the galaxy.
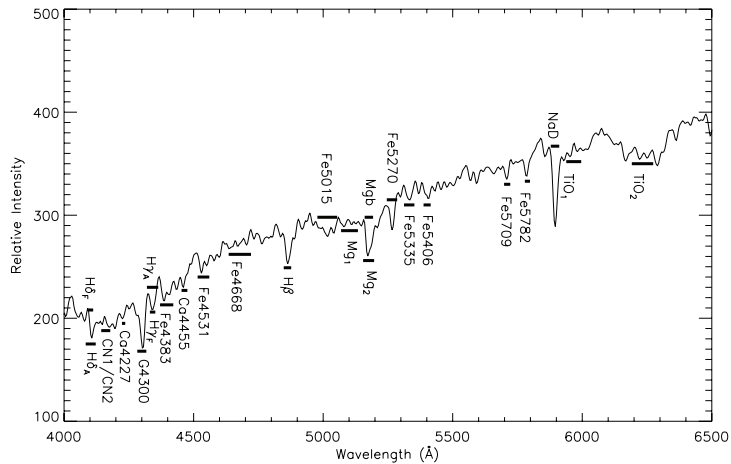

Fig. 3 Spectrum of GC B023 in our sample, with the index bandpasses of all the absorption Lick indices defined in Worthey et al. (1994) and Worthey & Ottaviani (1997) marked as thick horizontal lines. As we can see, the index bandpasses for CN1 and CN2 are the same and the only difference is the pseudocontinua coverage.

Table 3 Lick Absorption Line Indices of Our Sample GCs

Indices	MCGC2	MCGC3	B514	MCGC5	B298	H12	B019	B020	B023	EXT08	B517
Hδ_A (Å)	−2.297	3.038	2.526	3.450	4.520	3.331	1.640	1.592	0.719	4.054	2.797
error	0.351	0.270	0.315	0.294	0.532	0.249	0.309	0.347	0.228	0.322	0.258
Hδ_F (Å)	0.154	2.258	1.916	2.839	2.775	1.977	0.661	1.136	0.589	2.497	−0.358
error	0.237	0.260	0.256	0.307	0.362	0.213	0.233	0.256	0.174	0.215	0.204
CN1 (mag)	0.037	−0.084	−0.095	−0.137	−0.104	−0.069	−0.039	−0.056	0.031	−0.142	−0.097
error	0.011	0.008	0.007	0.009	0.011	0.007	0.007	0.010	0.005	0.008	0.006
CN2 (mag)	0.097	0.015	−0.013	−0.060	0.029	−0.023	0.033	0.013	0.082	−0.066	−0.022
error	0.015	0.022	0.015	0.019	0.024	0.017	0.014	0.012	0.011	0.020	0.011
Ca4227 (Å)	0.358	0.383	0.000	0.119	0.340	0.582	0.388	0.170	0.230	0.127	0.085
error	0.219	0.093	0.040	0.110	0.118	0.148	0.097	0.076	0.074	0.047	0.156
G4300 (Å)	1.416	1.577	1.381	3.088	0.954	1.221	3.117	2.871	3.534	0.272	1.901
error	0.482	0.323	0.225	0.396	0.254	0.393	0.319	0.448	0.414	0.225	0.172
Hγ_A (Å)	−0.747	1.064	0.954	−1.626	2.603	−0.834	−4.478	−6.141	−5.271	1.746	−0.215
error	0.489	0.277	0.249	0.284	0.206	0.339	0.394	0.381	0.400	0.288	0.239
Hγ_F (Å)	1.747	1.364	1.307	0.339	1.346	1.022	−0.321	−0.788	−0.056	1.924	0.923
error	0.254	0.199	0.167	0.252	0.133	0.257	0.157	0.179	0.168	0.181	0.179
Fe4383 (Å)	−0.202	−0.202	−0.520	−0.654	0.240	0.816	1.957	2.439	3.115	0.357	0.244
error	0.543	0.406	0.286	0.240	0.566	0.241	0.335	0.375	0.379	0.199	0.301
Ca4455 (Å)	0.321	0.399	0.055	0.243	1.309	0.391	0.530	0.291	0.601	0.118	0.810
error	0.252	0.224	0.078	0.078	0.260	0.121	0.183	0.099	0.127	0.030	0.219
Fe4531 (Å)	0.169	0.300	0.287	0.823	0.298	−0.642	1.929	1.711	1.582	0.281	2.319
error	0.545	0.212	0.120	0.223	0.208	0.167	0.232	0.348	0.155	0.111	0.237
Fe4668 (Å)	−1.582	−0.848	2.038	−1.400	0.662	−2.585	2.566	1.162	0.848	−0.498	1.024
error	0.405	0.289	0.251	0.336	0.433	0.335	0.347	0.181	0.214	0.080	0.311
Hβ (Å)	2.212	1.794	2.250	2.269	2.308	3.082	2.037	1.791	1.526	2.583	3.148
error	0.187	0.209	0.211	0.243	0.254	0.305	0.336	0.242	0.214	0.219	0.290
Fe5015 (Å)	−0.557	1.044	1.506	1.305	−0.388	2.170	3.209	3.281	2.242	0.342	1.903
error	0.386	0.216	0.144	0.198	0.137	0.359	0.384	0.304	0.167	0.076	0.271
Mg1 (mag)	0.054	0.004	−0.007	−0.003	0.011	0.014	0.034	0.017	0.032	0.015	0.001
error	0.005	0.001	0.001	0.002	0.002	0.002	0.002	0.003	0.002	0.001	0.002
Mg2 (mag)	0.053	0.027	0.028	0.027	0.033	0.036	0.121	0.102	0.119	0.004	0.044
error	0.004	0.004	0.003	0.004	0.002	0.002	0.008	0.006	0.006	0.002	0.004
Mgb (Å)	0.506	0.415	0.518	1.370	0.109	0.731	2.392	2.178	1.927	0.088	0.962
error	0.165	0.140	0.098	0.156	0.093	0.105	0.241	0.214	0.163	0.063	0.164
Fe5270 (Å)	0.202	0.409	0.919	0.339	−0.185	0.148	1.345	1.900	1.526	0.225	1.618
error	0.270	0.086	0.140	0.111	0.137	0.103	0.184	0.252	0.205	0.043	0.194
Fe5335 (Å)	−0.391	0.529	0.166	1.082	0.703	−0.221	1.014	0.979	1.187	0.439	0.730
error	0.217	0.093	0.091	0.187	0.125	0.101	0.190	0.195	0.177	0.074	0.177
Fe5406 (Å)	0.481	−0.388	−0.061	0.282	−0.235	0.234	0.993	0.557	0.730	0.224	0.108
error	0.268	0.193	0.091	0.108	0.144	0.115	0.166	0.092	0.113	0.059	0.101
Fe5709 (Å)	−0.045	0.021	0.008	0.325	−0.416	0.286	0.351	0.021	0.483	0.050	0.025
error	0.082	0.041	0.020	0.061	0.103	0.107	0.075	0.078	0.087	0.028	0.111
Fe5782 (Å)	0.334	0.142	0.177	0.239	0.275	−0.143	0.311	0.186	0.512	0.103	−0.128
error	0.105	0.028	0.053	0.062	0.094	0.077	0.064	0.053	0.097	0.029	0.086
NaD (Å)	1.025	1.492	1.175	1.446	1.663	1.559	3.491	2.490	3.642	0.744	0.215
error	0.113	0.121	0.094	0.164	0.192	0.150	0.399	0.254	0.380	0.083	0.070
TiO1 (mag)	0.038	0.004	0.007	0.015	−0.008	0.009	0.036	0.024	0.046	0.012	0.002
error	0.003	0.002	0.002	0.001	0.003	0.002	0.001	0.002	0.001	0.001	0.004
TiO2 (mag)	−0.009	0.011	0.002	0.016	0.019	−0.024	0.062	0.050	0.064	0.009	0.015
error	0.003	0.001	0.001	0.001	0.002	0.002	0.001	0.001	0.001	0.001	0.002

and CN2 (Worthey et al. 1994; Worthey & Ottaviani 1997), we find that their index bandpasses are totally the same and the only difference is the pseudocontinua coverage.

A simple way to estimate the metallicity is by calculating it from the combination of absorption line indices Mg and Fe. Galleti et al. (2009) provide the method to measure the metallicity from [MgFe], which is defined as [MgFe] = $\sqrt{\mathrm{Mgb}\langle\mathrm{Fe}\rangle}$, with $\langle\mathrm{Fe}\rangle$ = (Fe5270+Fe5335)/2. Thus, the

Table 4 χ^2-minimization Fitting Results using Thomas et al. (2011) Models with Cassisi et al. (1997) and Padova Stellar Tracks

ID	$[\mathrm{Fe/H}]_{[\mathrm{MgFe}]}$	$[\mathrm{Fe/H}]_{\mathrm{Cas}}$	$\mathrm{Age}_{\mathrm{Cas}}(\mathrm{Gyr})$	$[\alpha/\mathrm{Fe}]_{\mathrm{Cas}}$	$[\mathrm{Fe/H}]_{\mathrm{Pad}}$	$\mathrm{Age}_{\mathrm{Pad}}(\mathrm{Gyr})$	$[\alpha/\mathrm{Fe}]_{\mathrm{Pad}}$
MCGC2	-2.32 ± 0.28	$-1.53^{+0.28}_{-0.18}$	$13.60^{+0.40}_{-0.50}$	$0.46^{+0.02}_{-0.76}$	$-1.44^{+0.19}_{-0.18}$	$13.60^{+0.50}_{-1.00}$	$0.50^{+0.00}_{-0.80}$
MCGC3	-2.09 ± 0.13	$-1.80^{+0.09}_{-0.18}$	$13.60^{+0.50}_{-2.30}$	$0.50^{+0.00}_{-0.47}$	$-1.80^{+0.18}_{-0.18}$	$13.60^{+0.80}_{-2.90}$	$0.50^{+0.00}_{-0.50}$
B514	-2.00 ± 0.12	$-1.89^{+0.09}_{-0.18}$	$13.60^{+0.40}_{-0.60}$	$0.50^{+0.00}_{-0.38}$	$-1.89^{+0.18}_{-0.18}$	$13.60^{+1.30}_{-2.70}$	$0.50^{+0.00}_{-0.35}$
MCGC5	-1.56 ± 0.18	$-1.53^{+0.18}_{-0.18}$	$13.60^{+1.40}_{-0.60}$	$0.50^{+0.00}_{-0.35}$	$-1.44^{+0.09}_{-0.18}$	$13.60^{+0.60}_{-2.40}$	$0.50^{+0.00}_{-0.29}$
B298	-2.38 ± 0.13	$-2.07^{+0.18}_{-0.09}$	$13.60^{+0.50}_{-3.00}$	$0.50^{+0.00}_{-0.65}$	$-2.07^{+0.18}_{-0.18}$	$13.60^{+0.60}_{-3.40}$	$0.50^{+0.00}_{-0.62}$
H12	-2.38 ± 0.24	$-1.80^{+0.18}_{-0.18}$	$13.60^{+1.40}_{-1.70}$	$0.50^{+0.00}_{-0.26}$	$-1.71^{+0.18}_{-0.18}$	$14.80^{+0.20}_{-4.20}$	$0.50^{+0.00}_{-0.20}$
B019	-0.98 ± 0.26	$-0.74^{+0.10}_{-0.20}$	$13.50^{+0.80}_{-2.70}$	$0.48^{+0.02}_{-0.33}$	$-0.53^{+0.10}_{-0.10}$	$7.70^{+6.30}_{-0.80}$	$0.48^{+0.02}_{-0.36}$
B020	-0.91 ± 0.26	$-0.94^{+0.20}_{-0.10}$	$13.70^{+0.30}_{-0.50}$	$0.44^{+0.06}_{-0.41}$	$-0.94^{+0.10}_{-0.10}$	$13.60^{+0.30}_{-0.30}$	$0.50^{+0.00}_{-0.35}$
B023	-1.03 ± 0.21	$-0.84^{+0.10}_{-0.10}$	$13.60^{+0.50}_{-0.60}$	$0.34^{+0.16}_{-0.37}$	$-0.74^{+0.10}_{-0.20}$	$13.20^{+0.20}_{-1.50}$	$0.40^{+0.10}_{-0.34}$
EXT8	-2.38 ± 0.09	$-2.07^{+0.09}_{-0.18}$	$13.50^{+0.60}_{-4.30}$	$0.50^{+0.00}_{-0.80}$	$-2.07^{+0.09}_{-0.18}$	$13.50^{+1.40}_{-4.50}$	$0.50^{+0.00}_{-0.80}$
B517	-1.49 ± 0.20	$-1.53^{+0.09}_{-0.18}$	$13.60^{+1.40}_{-0.60}$	$0.00^{+0.50}_{-0.30}$	$-1.53^{+0.18}_{-0.09}$	$13.60^{+0.60}_{-1.70}$	$0.00^{+0.50}_{-0.30}$

Cas: fitting with the model evolutionary tracks of Cassisi et al. (1997); Pad: fitting with the model evolutionary tracks of Padova.

metallicity can be derived from the formula below,

$$[\mathrm{Fe/H}]_{[\mathrm{MgFe}]} = -2.563 + 1.119[\mathrm{MgFe}] - 0.106[\mathrm{MgFe}]^2 \pm 0.15. \tag{1}$$

The uncertainty of the $[\mathrm{Fe/H}]_{[\mathrm{MgFe}]}$ was estimated with the equation in the following,

$$\sigma^2_{[\mathrm{Fe/H}]} = 1.119^2 \sigma^2_{[\mathrm{MgFe}]} + 4 \times 0.106^2 [\mathrm{MgFe}]^2 \sigma^2_{[\mathrm{MgFe}]}. \tag{2}$$

All metallicity $[\mathrm{Fe/H}]_{[\mathrm{MgFe}]}$ values derived from [MgFe] and the associated uncertainty determinations are listed in Col. (2) of Table 4. It is obvious that all the metallicity values derived from the line index [MgFe] agree well with those from the model fitting method.

4 FITTING, ANALYSIS AND RESULTS

4.1 Model Description

Thomas et al. (2003) provided stellar population models including Lick absorption line indices for various elemental-abundance ratios, covering ages from 1 to 15 Gyr and metallicities from 1/200 to $3.5\times$ solar abundance. These models are based on the standard models of Maraston (1998), with input stellar evolutionary tracks from Cassisi et al. (1997) and Bono et al. (1997) and a Salpeter (1955) stellar initial mass function. Thomas et al. (2004) improved the models by including higher-order Balmer absorption-line indices. They found that these Balmer indices are very sensitive to changes in the α/Fe ratio for supersolar metallicities. The latest stellar population model for the Lick absorption-line indices (Thomas et al. 2011) is an improvement on Thomas et al. (2003) and Thomas et al. (2004). They were derived from the MILES stellar library, which provides a higher spectral resolution appropriate for MILES and SDSS spectroscopy, as well as flux calibration. The models cover ages from 0.1 to 15 Gyr, [Fe/H] from -2.25 to 0.67 dex, and [α/Fe] from -0.3 to 0.5 dex. In our work, we fitted our absorption indices based on the models of Thomas et al. (2011), by using the two sets of stellar evolutionary tracks provided from, i.e. Cassisi et al. (1997) and Padova.

4.2 Fitting with Stellar Population Models and the Results

As Caldwell et al. (2009) demonstrated, the χ^2−minimization method for many diagnostic lines is more reliable for extracting the ages than the two absorption line index diagram method. Furthermore, we have measured 25 different types of Lick line indices listed in Table 3, all of which were used for the fitting procedure, so the results should be much more reliable and accurate. Since Thomas et al. (2011) provide only 20 ages, 6 [Fe/H] values and 4 [α/Fe], it is necessary to interpolate the original models to the higher-resolution models for our needs. We carried out the cubic spline interpolations, using equal step lengths, to obtain a grid of 150 ages from 0.1 to 15 Gyr, 31 [Fe/H] values from −2.25 to 0.67 dex and 51 [α/Fe] from −0.3 to 0.5 dex, which makes the model more accurate and more helpful for our following statistics. Therefore, the ages (t), metallicities [Fe/H], and [α/Fe] were determined at the same time by comparing the interpolated stellar population models with the spectral-energy distributions from our photometry by employing the χ^2−minimization method, i.e.,

$$\chi^2_{\min}(t, \mathrm{Fe/H}, \alpha/\mathrm{Fe}) = \min \left[\sum_{i=1}^{25} \left(\frac{L^{\mathrm{obs}}_{\lambda_i} - L^{\mathrm{mod}}_{\lambda_i}}{\sigma_i} \right)^2 \right], \tag{3}$$

where $L^{\mathrm{mod}}_{\lambda_i}(t, \mathrm{Fe/H}, \alpha/\mathrm{Fe})$ is the ith Lick line index in the stellar population model for age t, metallicity [Fe/H] and [α/Fe], while $L^{\mathrm{obs}}_{\lambda_i}$ represents the observed Lick line indices from our measurements and the errors estimated in our fitting are given as follows,

$$\sigma_i^2 = \sigma^2_{\mathrm{obs},i} + \sigma^2_{\mathrm{mod},i}. \tag{4}$$

Here, $\sigma_{\mathrm{obs},i}$ is the observational uncertainty and $\sigma_{\mathrm{mod},i}$ is the uncertainty associated with the models of Thomas et al. (2011). We combined the two uncertainties together in our fitting.

From Table 4, we found that the [Fe/H], the ages and the [α/Fe] derived from either Cassisi et al. (1997) or from the Padova tracks of the models are basically the same, suggesting that our fitting results are consistent with each other. Moreover, the ages constrained in our work are in good agreement with those from previous work in Table 4, implying that our fitting method is reliable. In addition, it is worth noting that all of our sample GCs, most of which are located in the galaxy's halo, are older than 10 Gyr, indicating that these clusters formed at the very beginning of the galaxy's formation. We also find that the metallicity derived from the absorption-line index [MgFe] (in Col. (2)) is consistent with that fitted with two different tracks of the model (in Cols. (3) and (6)). Previously, Galleti et al. (2005) estimated the metallicity of B514 with [Fe/H]= −1.8 ± 0.3, and RBC v.4 lists the metallicity for B514 [Fe/H]= −2.06 ± 0.16, for B298 [Fe/H]= −1.78 ± 0.22, for B019 [Fe/H]= −0.74 ± 0.15, for B020 [Fe/H]= −0.83 ± 0.07 and for B023 [Fe/H]= −0.91 ± 0.14. All these previous measurements are in good agreement with our estimates in Table 4, indicating our method and results are reliable. For consistency, in the subsequent analysis, we adopted the ages and metallicities from the Thomas et al. (2011) + Cassisi et al. (1997) track of the predictive model.

4.3 Metallicity Properties of the Outer Halo

Metal abundance is one of the most important properties of star clusters for understanding the formation and enrichment processes of their host galaxy. For instance, the halo stars and clusters should feature large-scale metallicity gradients if the enrichment timescale is shorter than the collapse time, which may be due to the galaxy's formation being a consequence of a monolithic, dissipative and rapid collapse of a single massive, nearly spherical, spinning gas cloud (Eggen et al. 1962; Barmby et al. 2000). On the other hand, Searle & Zinn (1978) presented a chaotic scheme for early galactic evolution, when the loosely bound pre-enriched fragments merge with the protogalaxy during a very long period of time, in which case a more homogeneous metallicity distribution should develop. Most galaxies are thought to have formed through a combination of these scenarios.

A lot of previous work attempted to find the clues of formation and evolution for galaxy M31 through studying the metallicity distribution of its GC system. Huchra et al. (1991); Ashman & Bird (1993); Barmby et al. (2000); Perrett et al. (2002); Fan et al. (2008) found that the metal-rich GCs are statistically more concentrated toward the center of the galaxy, while their metal-poor counterparts are more spatially extended in the halo. Furthermore, there are also many studies to investigate whether or not a radial metallicity gradient exists for the M31 star cluster system. van den Bergh (1969); Huchra et al. (1982) showed that there is little or no evidence for a general radial metallicity gradient for GCs within a radius of 50 arcmin. However, studies including Huchra et al. (1991); Perrett et al. (2002); Fan et al. (2008) support the possible existence of a radial metallicity gradient for the metal-poor M31 GCs, although the slope is not very significant. Perrett et al. (2002) suggest that the gradients are -0.017 and -0.015 dex arcmin^{-1} for the full sample and inner metal-poor clusters respectively. More recently, Fan et al. (2008) found that the slope is -0.006 and -0.007 dex arcmin^{-1} for the metal-poor subsample and whole sample respectively while the slope approaches zero for the metal-rich subsample. Nevertheless, all these studies are based on GCs that are located relatively close to the center of the galaxy, usually at projected radii of less than 100 arcmin. In our work, we extended the radial coverage to a radius of $r_{\rm p} \sim 117$ kpc, which corresponds to ~ 510 arcmin, to check if the previous findings are correct at a much larger distance from the galaxy's center.

For the purpose of better investigating the metallicity distribution/spatial gradient, we enlarged the metallicity sample by merging the metallicity of our measurements with the published spectroscopic metallicity from Huchra et al. (1991); Barmby et al. (2000); Perrett et al. (2002); Galleti et al. (2009); Caldwell et al. (2011) together with those from CMD fittings (Mackey et al. 2006, 2007, 2010). For the published data, if the metallicity from different works overlapped with each other, the one with smaller uncertainty in the data set will supersede the larger one and the spectroscopic data set will supersede the one derived from CMD fitting. In total, we have a metallicity sample of 384 entries.

Figure 4 shows metallicity as a function of projected radius from the galaxy center for all confirmed M31 clusters (top) and the halo clusters only (bottom) in the unit of kpc. In the top panel, open triangles with error bars represent the spectroscopic metallicities from the published measurements of Huchra et al. (1991); Barmby et al. (2000); Perrett et al. (2002); Galleti et al. (2009); Caldwell et al. (2011) as well as the metallicities from CMD fitting from Mackey et al. (2006, 2007, 2010) while the green filled triangles with error bars are our spectroscopic measurements. The solid line is a linear fit to all the data points, with a slope of -0.028 ± 0.001 dex kpc^{-1}, corresponding to -0.007 dex arcmin^{-1}. The fit results are similar to those given by previous work (see, Perrett et al. 2002; Fan et al. 2008), which are based on the cluster sample within projected radii $r_{\rm p} < 100$ arcmin (~ 23 kpc). Thus, our work tentatively supports the notion that a radial metallicity gradient may exist out to a projected radius of ~ 117 kpc by merging the published metallicities. In other words, we updated the results with the new sample which extends to M31's most remote outer halo. Since the aim of our work is to study the nature of M31's halo, we would like to focus on the metallicity gradient of halo clusters. In the bottom panel, we only plot the halo clusters, which are defined in Figure 1. A least-squares fit yields the slope of -0.018 ± 0.001 dex kpc^{-1}. Therefore, it can be seen that the metallicity gradient seems to exist for the halo clusters, although it is not significant.

Furthermore, it is noted that in Figure 4, the metallicity gradient for the clusters located in the outer halo with $r_{\rm p} > 25$ kpc is not significant. Thus, we show metallicity as a function of projected radius for only the outer halo clusters with $r_{\rm p} > 25$ kpc in Figure 5. A least-squares linear fit for all the data shows the slope is -0.010 ± 0.002 dex kpc^{-1} (the solid line). However, if G001 is excluded, the slope turns out to be -0.004 ± 0.002 dex kpc^{-1} (the dashed line), which is much shallower than that in Figure 4. It may suggest that the metallicity gradient is not significant for the outer halo clusters in M31. Very recently, Huxor et al. (2011) investigated the metallicity gradient for 15 halo CGs to $r_{\rm p} = 117$ kpc with the metallicity derived from CMD fitting (Mackey et al. 2006,
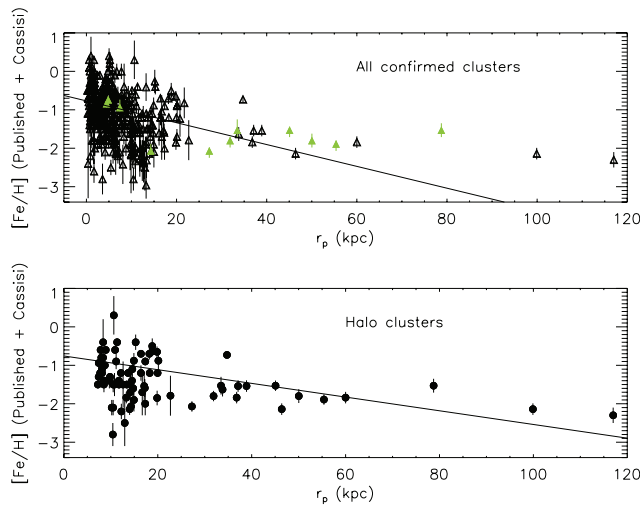
Fig. 4 [Fe/H] versus projected radius from the galaxy center for M31 GCs. The solid line refers to a linear fit for all the data. *Top*: All the confirmed clusters. The open triangles with error bars represent published metallicities while the filled triangles with error bars are our measurements. *Bottom*: Halo clusters only. All the clusters are marked with filled circles.
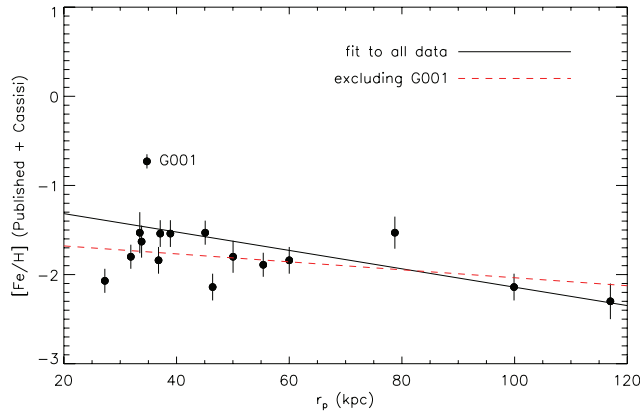

Fig. 5 [Fe/H] versus projected radius from the galaxy center for outer halo GCs, whose $r_p > 25$ kpc from the center of the galaxy. The slope of the fitting for all the data is -0.010 ± 0.002 dex kpc^{-1}. However, if G001 is excluded, the slope turns out to be -0.004 ± 0.002 dex kpc^{-1}.

2007, 2010) and the authors found that the metallicity gradient becomes insignificant if one halo GC H14 is excluded, as shown in their figure 6. We found that our result is consistent with the previous finding of Huxor et al. (2011).

5 DISCUSSION AND SUMMARY

In our work, we carried out spectroscopic observations of 11 confirmed globular clusters of M31 with the OMR spectrograph and a PI 1340×400 CCD detector on the 2.16 m telescope at the Xinglong site of NAOC during 2010 September 10–13. Since our aim is to study the nature of the halo of M31,

we selected the bright confirmed clusters, nine of which are located in the halo, out to a projected radius of 78.75 kpc from the galactic center.

For all our sample clusters, we measured all types of Lick absorption-line indices (see the definitions in Worthey et al. 1994; Worthey & Ottaviani 1997) as well as radial velocities. We found that most GCs of our sample are distinct from the HI rotation curve of galaxy M31, especially for B514, MCGC5, H12 and B517, suggesting that most of our sample clusters do not have a kinematic association with the star-forming young disk of the galaxy.

Since Caldwell et al. (2009) demonstrated that the χ^2-minimization method for many diagnostic lines is more reliable for extracting the ages than the line index plot, in our work we applied the χ^2-minimization method to separately fit the line indices with the updated stellar population model (Thomas et al. 2011) with two different tracks of Cassisi and Padova. The fitting results show that all our sample clusters are older than 10 Gyr and most of them are metal-poor ($-2.38 \leq$ [Fe/H] ≤ -0.91 dex).

In order to enlarge our sample, we merged the spectroscopic metallicity of our work with previously published ones, extending the cluster sample out to a projected radius of 117 kpc from the galaxy's center. We found the metallicity gradient for all the confirmed clusters exists with a slope of -0.028 ± 0.001 dex kpc^{-1}. However, the slope turns out to be -0.018 ± 0.001 dex kpc^{-1} for all the halo clusters, which is much shallower. If we only consider the outer halo clusters with $r_{\rm p} > 25$ kpc, the slope becomes -0.010 ± 0.002 dex kpc^{-1} and if one cluster G001 is excluded from the outer halo sample, the slope could even be -0.004 ± 0.002 dex kpc^{-1}. Thus, we conclude that metallicity gradient for M31 outer halo clusters is not significant, which agrees well with previous findings. This result may imply that for galaxy M31's formation, the "rapid collapsing" scenario is supported inside the inner halo while the "fragments merging" scenario is consistent in the outer halo of the galaxy beyond 25 kpc from the center. It seems that the combination of the two scenarios could best explain galaxy formation. However, we still need more observations and further study to definitively confirm these conclusions.

It is interesting to note that the halo of galaxy M31 might be divided into two parts (by combining the Huxor data): the inner halo and the outer halo from our study. The nature of the two parts of the halo seems to be different in terms of metallicity gradients of the star clusters, which may be due to the different formation mechanisms of the two parts. Just like the Milky Way halo from the SDSS/SEGUE data, the Milky Way halo could be divided into two parts with different metallicity properties based on the observations of a large sample of halo stars. Therefore, it seems that galaxy M31 and our Galaxy have more similarities than we expected. However, more observational data are required for further study in the future.

References

Ashman, K. M., & Bird, C. M. 1993, AJ, 106, 2281
Barmby, P., Holland, S., & Huchra, J. P. 2002, AJ, 123, 1937
Barmby, P., & Huchra, J. P. 2001, AJ, 122, 2458
Barmby, P., Huchra, J. P., Brodie, J. P., et al. 2000, AJ, 119, 727
Bono, G., Caputo, F., Cassisi, S., Castellani, V., & Marconi, M. 1997, ApJ, 489, 822
Caldwell, N., Harding, P., Morrison, H., et al. 2009, AJ, 137, 94

Caldwell, N., Schiavon, R., Morrison, H., Rose, J. A., & Harding, P. 2011, AJ, 141, 61
Cardiel, N., Gorgas, J., Cenarro, J., & Gonzalez, J. J. 1998, A&AS, 127, 597
Carignan, C., Chemin, L., Huchtmeier, W. K., & Lockman, F. J. 2006, ApJ, 641, L109
Cassisi, S., Castellani, M., & Castellani, V. 1997, A&A, 317, 108
Djorgovski, S. G., Gal, R. R., McCarthy, J. K., et al. 1997, ApJ, 474, L19
Eggen, O. J., Lynden-Bell, D., & Sandage, A. R. 1962, ApJ, 136, 748
Fan, Z., Ma, J., de Grijs, R., & Zhou, X. 2008, MNRAS, 385, 1973
Fusi Pecci, F., Battistini, P., Bendinelli, O., et al. 1994, A&A, 284, 349
Galleti, S., Bellazzini, M., Buzzoni, A., Federici, L., & Fusi Pecci, F. 2009, A&A, 508, 1285
Galleti, S., Bellazzini, M., Federici, L., Buzzoni, A., & Fusi Pecci, F. 2007, A&A, 471, 127
Galleti, S., Bellazzini, M., Federici, L., & Fusi Pecci, F. 2005, A&A, 436, 535
Galleti, S., Federici, L., Bellazzini, M., Buzzoni, A., & Fusi Pecci, F. 2006, A&A, 456, 985
Galleti, S., Federici, L., Bellazzini, M., Fusi Pecci, F., & Macrina, S. 2004, A&A, 416, 917
Hammer, F., Puech, M., Chemin, L., Flores, H., & Lehnert, M. D. 2007, ApJ, 662, 322
Hou, J., Yin, J., Boissier, S., et al. 2009, in IAU Symposium, vol. 254, eds. J. Andersen, J. Bland-Hawthorn, &
    B. Nordström, 27
Huchra, J., Stauffer, J., & van Speybroeck, L. 1982, ApJ, 259, L57
Huchra, J. P., Brodie, J. P., & Kent, S. M. 1991, ApJ, 370, 495
Huxor, A., Tanvir, N. R., Irwin, M., et al. 2004, in ASPC Series 327, Satellites and Tidal Streams, eds. F. Prada,
    D. Martinez Delgado, & T. J. Mahoney (San Francisco: ASP), 118
Huxor, A. P. 2006, Ph.D. thesis, Univ. Hertfordshire
Huxor, A. P., Ferguson, A. M. N., Tanvir, N. R., et al. 2011, MNRAS, 414, 770
Huxor, A. P., Tanvir, N. R., Irwin, M. J., et al. 2005, MNRAS, 360, 1007
Jester, S., Schneider, D. P., Richards, G. T., et al. 2005, AJ, 130, 873
Ma, J., Wu, Z., Wang, S., et al. 2010, PASP, 122, 1164
Mackey, A. D., Ferguson, A. M. N., Irwin, M. J., et al. 2010, MNRAS, 401, 533
Mackey, A. D., Huxor, A., Ferguson, A. M. N., et al. 2006, ApJ, 653, L105
Mackey, A. D., Huxor, A., Ferguson, A. M. N., et al. 2007, ApJ, 655, L85
Macri, L. M., Calzetti, D., Freedman, W. L., et al. 2001, ApJ, 549, 721
Maraston, C. 1998, MNRAS, 300, 872
Massey, P., Strobel, K., Barnes, J. V., & Anderson, E. 1988, ApJ, 328, 315
McConnachie, A. W., Irwin, M. J., Ferguson, A. M. N., et al. 2005, MNRAS, 356, 979
Peacock, M. B., Maccarone, T. J., Knigge, C., et al. 2010, MNRAS, 402, 803
Peng, E. W., Côté, P., Jordán, A., et al. 2006, ApJ, 639, 838
Perina, S., Cohen, J. G., Barmby, P., et al. 2010, A&A, 511, A23
Perrett, K. M., Bridges, T. J., Hanes, D. A., et al. 2002, AJ, 123, 2490
Racine, R. 1991, AJ, 101, 865
Rich, R. M., Corsi, C. E., Cacciari, C., et al. 2005, AJ, 129, 2670
Salpeter, E. E. 1955, ApJ, 121, 161
Searle, L., & Zinn, R. 1978, ApJ, 225, 357
Stanek, K. Z., & Garnavich, P. M. 1998, ApJ, 503, L131
Thomas, D., Maraston, C., & Bender, R. 2003, MNRAS, 339, 897
Thomas, D., Maraston, C., & Johansson, J. 2011, MNRAS, 412, 2183
Thomas, D., Maraston, C., & Korn, A. 2004, MNRAS, 351, L19
van den Bergh, S. 1969, ApJS, 19, 145
Worthey, G., Faber, S. M., Gonzalez, J. J., & Burstein, D. 1994, ApJS, 94, 687
Worthey, G., & Ottaviani, D. L. 1997, ApJS, 111, 377
Yin, J., Hou, J. L., Prantzos, N., et al. 2009, A&A, 505, 497